Layered Ruddlesden−Popper Manganese Oxides: Synthesis and Cation Ordering

P. D. Battle,* M. A. Green, N. S. Laskey, J. E. Millburn, L. Murphy, M. J. Rosseinsky,* S. P. Sullivan, and J. F. Vente

Inorganic Chemistry Laboratory, University of Oxford, South Parks Road, Oxford, OX1 3QR U.K.

Received July 26, 1996. Revised Manuscript Received September 25, 1996[⊗]

The preparation and crystal structures of the $n = 2$ Ruddlesden−Popper phases $Sr_{2-x}Ln_{1+x}Mn_2O_7$ ($0 \le x \le 0.5$, Ln = La, Pr, Nd, Sm, Eu, Gd, Tb, Dy, Ho, Y, and Er) are described. The crystal chemistry and stability of this structure is governed by the size of the lanthanide cation. Partial ordering of the Sr^{2+} and Ln^{3+} cations occurs between the two available A cation ($A = Ln^{3+}$, Sr^{2+}) sites, with the smaller lanthanides preferring the site in the rock-salt layer over that in the perovskite block. This ordering is almost complete for the small lanthanides (Tb−Er), and these ordered compounds can be prepared as single phases. Cation disorder in compounds of the larger lanthanides is accompanied by a subtle separation into two $n = 2$ Ruddlesden−Popper phases, which is apparent only upon detailed inspection of Rietveld refinements of the X-ray profiles. In these cases, the two-phase model is found to be superior to a single phase model with strain broadening included. For a particular lanthanide, both the ease of synthesis of single phases and the extent of cation ordering depend on the manganese oxidation state.

Introduction

There is an increasing interest in materials that show magnetoresistance, because of their use in magnetic information storage or as magnetic field sensors.[1] The efficiency of these devices is dependent on the percentage change of the resistance on application of an applied field. The magnetoresistance (MR), at a given temperature (T) and field (H), is defined as $MR(T,H) = \{[\rho(T,0) - \rho(T,H)]/\rho(T,H)\} \times 100\%$. Permalloy, which displays a magnetoresistance of 2−3% at room temperature in small applied magnetic fields, is currently used as a magnetoresistive sensor in reading heads for hard disk drives. An enhanced effect is seen in thin-film multilayers such as Cu/Co, where magnetoresistances of up to 150% are observed at 4.2 K (28% at room temperature) in 1−2 T fields.[2−4] Recently, attention has been focused on the mixed-valent lanthanide manganate perovskites which can show exceptionally high magnetoresistance, the magnitude of the effect being dependent on the size of the lanthanide cation, the manganese oxidation state, and the temperature.[5,6] The most common mechanism for this so-called "colossal magnetoresistance" (CMR) is the occurrence of an insulator-to-metal transition accompanying the onset of ferromagnetism. Application of fields of the order of 2−3 T at temperatures just above the Curie temperature (T_c) can drive the system into the metallic ferromagnetic state from the insulating paramagnetic one found in zero field, producing a very large negative magnetoresistance: 2.5×10^7% has been reported for $Sr_{0.05}Ca_{0.25}Pr_{0.7}MnO_{3-\delta}$ at 85 K in an applied field of 5 T.[7] The cation size dependence of T_c[8−10] is illustrated by $La_{0.67}Sr_{0.33}MnO_3$ ($T_c = 380$ K) and $Sm_{0.67}Sr_{0.33}MnO_3$ ($T_c = 100$ K).[11] This mechanism is also responsible for CMR in the Mn^{IV} pyrochlore $Tl_2Mn_2O_7$.[12] Large field-induced resistance changes also occur upon the melting of a "charge-ordered" Mn^{III}/Mn^{IV} superlattice at the metamagnetic transition of antiferromagnets with equal concentrations of Mn^{III} and Mn^{IV} such as $Ca_{0.5}Pr_{0.5}MnO_3$.[13] Cation substitution at the A site has recently seen CMR observed in this class of material in fields as low as 0.4 T.[14]

The majority of both the theoretical and experimental work has, until now, been focused on the three-dimensional structural limit. The perovskite is the $n = \infty$ end-member of the $A_{n+1}B_nO_{3n+1}$ Ruddlesden−Popper family, in which n 2D layers of BO_6 corner-sharing octahedra are joined along the stacking direction and separated by rock-salt AO layers. The $n = 1$ member is the two-dimensional K_2NiF_4 structure with a single layer of corner-sharing octahedra—$Sr_{1.2}La_{0.8}MnO_4$, with this structure is a spin glass with a freezing temperature of 20 K and does not display CMR.

[⊗] Abstract published in *Advance ACS Abstracts,* December 1, 1996.

(1) Heremans, J. *J. Phys. D* **1993**, *26*, 1149.
(2) Pankajavalli, R.; Sreedharan, O. M. *Mater. Lett.* **1995**, *24*, 247.
(3) Li, Y. Q.; Zhang, J.; Pombrik, S.; Dimascio, S.; Stevens, W.; Yan, Y. F.; Ong, N. P. *J. Mater. Res.* **1995**, *10*, 2166.
(4) Cherepanov, V. A.; Barkhatova, L. Y.; Petrov, A. N.; Voronin, V. I. *J. Solid State Chem.* **1995**, *118*, 53.
(5) Das, P. K.; Anand, S.; Das, R. P. *Int. J. Miner. Processing* **1995**, *43*, 99.
(6) Raveau, B.; Maignan, A.; Caignaert, V. *J. Solid State Chem.* **1995**, *117*, 424.
(7) Zeng, X. T.; Wong, H. K. *Appl. Phys. Lett.* **1995**, *66*, 3371.
(8) Maignan, A.; Caignaert, V.; Simon, C.; Hervieu, M.; Raveau, B. *J. Mater. Chem.* **1995**, 1089.
(9) Maignan, A.; Simon, C.; Caignaert, V.; Raveau, B. *Z. Phys. B* **1996**, *99*, 305.
(10) Mahendiran, R.; Tiwary, S. K.; Raychaudhuri, A. K.; Ramakrishnan, T. V.; Mahesh, R.; Rangavittal, N.; Rao, C. N. R. *Phys. Rev. B* **1996**, *53*, 3348.
(11) Kamata, H.; Yonemura, Y.; Mizusaki, J.; Tagawa, H.; Naraya, K.; Sasamoto, T. *J. Phys. Chem. Solids* **1995**, *56*, 943.
(12) Schiffer, P.; Ramirez, A. P.; Bao, W.; Cheong, S. W. *Phys. Rev. Lett.* **1995**, *75*, 3336.
(13) Tomioka, Y.; Asamitsu, A.; Kuwahara, H.; Moritomo, Y.; Tokura, Y. *Phys. Rev. B* **1996**, *53*, 1689.
(14) Kuwahara, H.; Tomioka, Y.; Moritomo, Y.; Asamitsu, A.; Kasai, M.; Kumai, R.; Tokura, Y. *Science* **1996**, *272*, 80.

S0897-4756(96)00398-5 CCC: $14.00

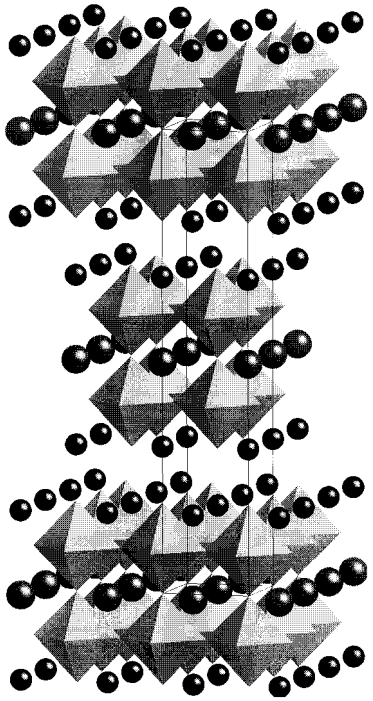

Figure 1. Crystal structure of the $n = 2$ Ruddlesden−Popper structure showing the two A cation sites. Large lightly colored circles represents the perovskite site cations, and the small dark circles represent the rock-salt site cations.

However, it has been demonstrated that the $n = 2$ Ruddlesden−Popper phase (Figure 1) $Sr_{1.8}La_{1.2}Mn_2O_7$[15] behaves in a similar manner to the $n = \infty$ perovskites: it undergoes a metal−insulator transition at a ferromagnetic Curie temperature (126 K) and has a large magnetoresistance in this temperature range. However, the change in dimensionality and resulting pronounced cation dependence of the electronic properties can produce physical properties which contrast strongly with the perovskite systems. Recently, it has been shown that colossal magnetoresistance in $Sr_{2-x}Nd_{1+x}Mn_2O_7$ is not associated with ferromagnetic behavior[16] and is therefore not readily explained by the double-exchange mechanism. In view of the sensitivity of the electronic properties to the structure, charge, and unit cell size,[17] we are investigating the $n = 2$ Ruddlesden−Popper series in detail. Previous work in this area[18−22] includes preparation of the phases $Sr_{2-x}Ln_{1+x}Mn_2O_7$ ($-1 \le x \le 0.5$ for Ln = La and $-1 \le x \le 0.4$ Ln = Nd, Sm, Gd)[20] and the observation of ferromagnetism in $Sr_{1.66}La_{1.33}Mn_2O_7$ with a Curie temperature of 130 K.[19,23] In this paper, we describe the synthesis and structural chemistry of the $n = 2$ Ruddlesden−Popper phases, $Sr_{2-x}Ln_{1+x}Mn_2O_7$ ($0 \le x \le 0.5$, Ln = La, Pr, Nd, Sm, Eu, Gd, Tb, Dy, Ho, Y, and Er).

Experimental Section

All materials were synthesized by solid-state reaction of stoichiometric quantities of MnO_2, $SrCO_3$, and the lanthanide oxide in an alumina boat. Lanthanide oxides were dried in a muffle furnace at 800 °C before use. The reaction mixtures were initially calcined at 800, 1000, and 1200 °C for 24 h each followed by grinding and pelletizing. The subsequent reaction conditions required to form the $n = 2$ RP structure free from contamination by other members of the Ruddlesden−Popper homologous series or the starting materials are summarized in Tables 1 and 2 for the $Sr_2LnMn_2O_7$ and $Sr_{2-x}Ln_{1+x}Mn_2O_7$ (Ln = Nd, Tb) series respectively. The $Sr_2LnMn_2O_7$ (Ln = lanthanide) phases with a formal manganese oxidation state of +3.5 were all successfully prepared in air. $Sr_{2-x}Ln_{1+x}Mn_2O_7$ phases with a formal manganese oxidation state of less than +3.5 (Ln = Tb) or +3.3 (Ln = Nd) required synthesis under flowing N_2 (BOC oxygen-free grade, used as received without drying). Attempts to determine the manganese oxidation state by iodometric titration were unsuccessful as the compounds did not dissolve in suitable solvents. Powder neutron diffraction measurements on $Sr_2NdMn_2O_7$ and $Sr_{1.9}Nd_{1.1}Mn_2O_7$ indicate that the compounds are stoichiometric in oxygen.[24] The progress of the syntheses was monitored after every firing stage by X-ray powder diffraction using a Phillips PW1710 powder diffractometer with a secondary graphite monochromator. X-ray powder diffraction data for structure analysis were collected with a Siemens D5000 diffractometer, using Cu $K\alpha_1$ radiation, in Bragg−Brentano geometry with the sample mounted on an amorphous silicon substrate. Rietveld refinement was performed with both the FullProf[25] code, which allows the incorporation into the refinement of anisotropic reflection broadening due to microstrain, and the GSAS suite of programs.[26] In the refinements, the background was fitted with a 6-term polynomial (FullProf) or a 10-term Chebyshev polynomial (GSAS): in both cases a pseudo-Voigt peak shape function was used.

Energy-dispersive X-ray analysis was carried out on a JEOL JEM-2000 FX 200 kV electron microscope with a Tracor Northern TN5500 spectrometer.

Results

Synthesis. The progress of the reactions was monitored closely by X-ray powder diffraction and Rietveld analysis. The ratio of the intensities of the reflections at $2\theta \approx 32.2°$ and 32.9° (which index as {110} and {105} from the $n = 2$ phase and {110} and {103} from the $n = 1$ phase, respectively) is critical in assessing which of the possible competing Ruddlesden−Popper structures are forming under a given set of reaction conditions. Monitoring with the lower resolution Phillips instrument proved a suitable method in determining the end-point of the reactions and the onset of decomposition into other phases. Several features were apparent from consideration of both the successful and unsuccessful syntheses: in the $Sr_2LnMn_2O_7$ case, the minimum temperature required for formation of pure phases uncontaminated by MnO or MnO_2 is 1350 °C, except for the Nd-containing samples, which only required 1300 °C. The preparation of the $n = 2$ RP structure for the smallest lanthanides which yielded the phase (Ln

(15) Chen, G.; Takenoshita, H.; Kasuya, M.; Satoh, H.; Kamegashira, N. *J. Alloys Compounds* **1995**, *228*, 127.
(16) Battle, P. D.; Blundell, S. J.; Green, M. A.; Hayes, W.; Honold, M.; Klehe, A. K.; Laskey, N. S.; Millburn, J. E.; Murphy, L.; Rosseinsky, M. J.; Samarin, N. A.; Singleton, J.; Sluchanko, N. E.; Sullivan, S. P.; Vente, J. F. *J. Phys. Condensed Matter* **1996**, *8*, L427.
(17) Battle, P. D.; Green, M. A.; Laskey, N. S.; Millburn, J. E.; Rosseinsky, M. J.; Sullivan, S. P.; Vente, J. F. *Chem. Commun.* **1996**, 767.
(18) Deschizeaux Cheruy, M. N.; Joubert, J. C. *J. Solid State Chem.* **1981**, *14*, 40.
(19) MacChesney, J. B.; Potter, J. F.; Sherwood, R. C. *J. Appl. Phys.* **1969**, *40*, 1243.
(20) Lamire, M.; Daoudi, A. *J. Solid State Chem.* **1984**, *55*, 327.
(21) Sharma, I. B.; Singh, D. *Proc. Indian Acad. Sci.* **1995**, *107*, 189.
(22) Moritomo, Y.; Asamitsu, A.; Kuwahara, H.; Tokura, Y. *Nature* **1996**, *380*, 141.
(23) Ram, R. A. M.; Ganguly, P.; Rao, C. N. R. *J. Solid State Chem.* **1987**, *70*, 82.
(24) Battle, P. D.; Green, M. A.; Laskey, N. S.; Millburn, J. E.; Radaelli, P. G.; Rosseinsky, M. J.; Sullivan, S. P.; Vente, J. F. *Phys. Rev. B* **1996**, *54*, 15967.
(25) Rodriguez-Cavajal, J. *FullProf*, Laboratoire Leon Brillouin, 1995.
(26) Larson, A. C.; von Dreele, R. B. *General Structure Analysis System*; Los Alamos National Laboratory, 1994, LAUR 86-748.

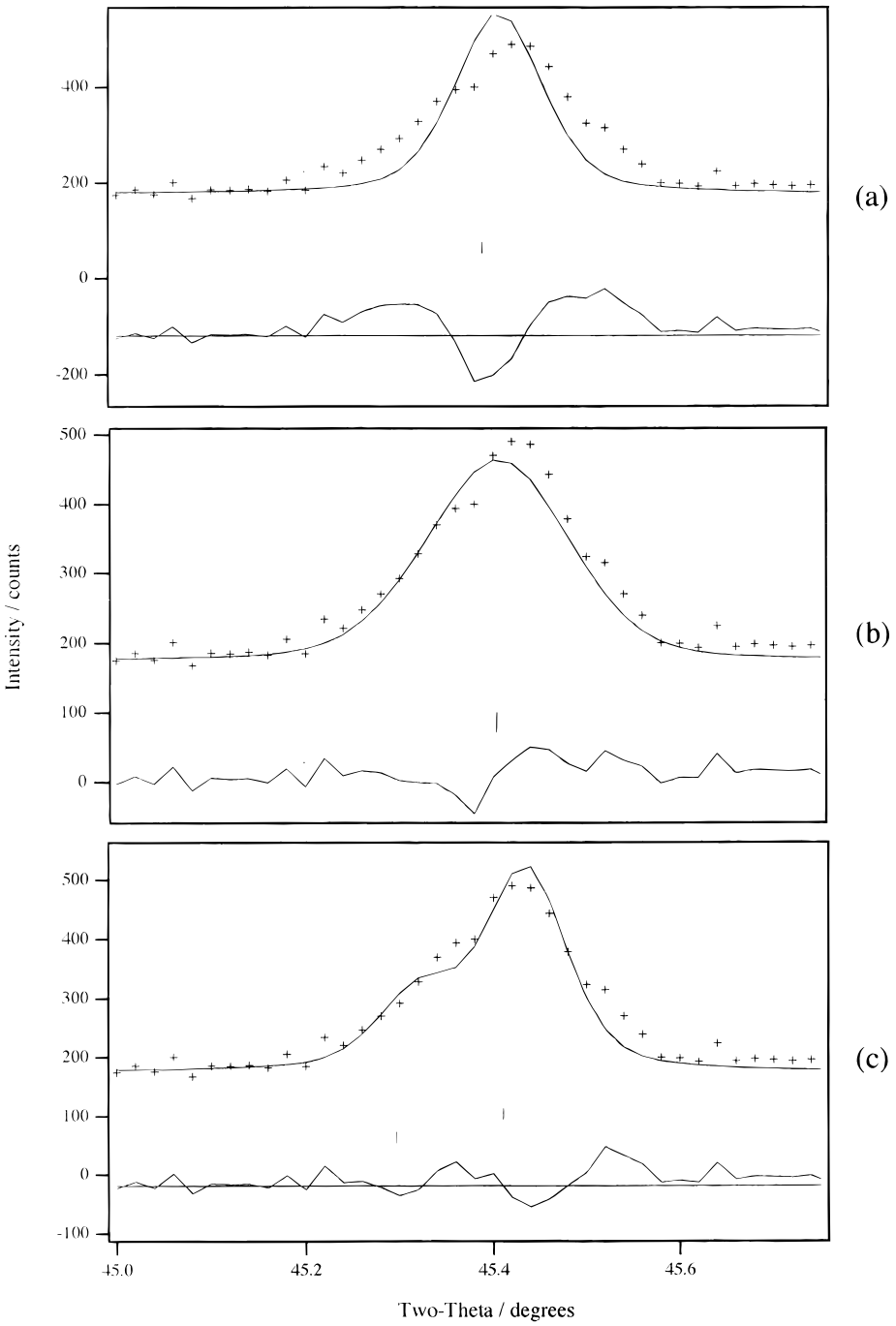

Figure 2. Rietveld fit to the {0 0 10} reflection of the $n = 2$ Ruddlesden−Popper structure for $Sr_2PrMn_2O_7$, using (a) a single-phase model ($wR_p = 8.32\%$, $R_p = 6.51\%$, and $\chi^2 = 1.25$), (b) a single-phase model with the inclusion of microstrain along the *c* axis ($wR_p = 8.25\%$, $R_p = 6.41\%$, and $\chi^2 = 1.24$) and (c) a two-phase model ($wR_p = 8.02\%$, $R_p = 6.36\%$, and $\chi^2 = 1.20$).

= Y, Er) required firing at 1450 °C to react the last traces of MnO_2, while the smaller Yb^{3+} cation did not appear to form the $n = 2$ Ruddlesden−Popper structure under these conditions. For Ln = Sm, firing at the higher temperature of 1450 °C resulted in decomposition of the $n = 2$ phase with the expulsion of MnO.

Structure. Rietveld refinement was carried out initially for all the compounds in the ideal tetragonal *I*4/*mmm* space group, giving lattice parameters of *a*, *b* ≈ 3.8 Å and *c* ≈ 20 Å with $Z = 2$. The structure is shown in Figure 1. In this space group, the A cations are distributed over two crystallographically independent sites: 4e 0 0 *z* and 2b 0 0 $^1/_2$, corresponding to cations in the rock-salt layers and the $n = 2$ perovskite block, respectively. Although both visual inspection and the numerical agreement indexes for single-phase Rietveld fits to the data for Ln = La−Tb indicated that a single $n = 2$ Ruddlesden−Popper phase had formed, careful inspection of individual reflections indicated that there were significant problems with the fit. For example, Figure 2a shows the single-phase Rietveld fit to the {0 0 10} reflection of $Sr_2PrMn_2O_7$. The calculated profile, although in excellent agreement with the observed data in other regions, clearly does not predict either the correct shape or intensity of this feature. The poorly fitted reflections all correspond to scattering vectors either parallel or close to the *c*-axis. Significantly, comparison of the refined peak-shape parameters indicates that the reflections are consistently considerably broader for the Ln = La−Gd samples than

for the phases formed by the smaller lanthanides. These observations are consistent with the observation of two-phase behavior in $Sr_2NdMn_2O_7$ upon refinement of high-resolution powder neutron diffraction data.[24]

A variety of models were used in order to improve the refinement while maintaining a single-phase model. The possibility of a distortion from the ideal tetragonal structure was tested. Neither a $\{\sqrt{2}a \times \sqrt{2}a \times c\}$ cell, as seen for example for $BaEu_2Mn_2O_7$[18] and $SrEu_2Fe_2O_7$,[27] nor an $\{a \times a \times 2c\}$ cell, as reported for $Sr_3Fe_2O_7$,[28] improved the fit in a Le Bail intensity extraction.[29] The FullProf[25] Rietveld refinement program was then employed with a microstrain broadening term along the *c* direction in order to model the excess width of $l \neq 0$ reflections, ascribing this to a distribution of repeat distances in this direction—an example of a successful application of this approach is the refinement of the crystal structure of $La_2NiO_{4.25}$, where the intercalation of oxygen into the K_2NiF_4 structure causes a distribution in the *c* parameter.[30] The profile fit and agreement indices improved upon the application of this model. However, for nonoverlapping reflections, such as the {0 0 10}, shown in Figure 2b, the reflection shape is still not well predicted. The fit was not improved by inclusion of other strain broadening parameters.

As the anomalous shapes of the {00*l*} reflections could not be modeled satisfactorily with the assumption of a single phase, we used a model containing two $n = 2$ Ruddlesden−Popper phases in which the profile parameters, isotropic thermal factors and site occupancies of the two phases were constrained to be the same but the lattice parameters and fractional coordinates were allowed to refine independently. This gave a marked improvement in the fit to the reflections which are poorly modeled in the single-phase fits. The fit to the {0 0 10} reflection in a two-phase Rietveld refinement, where both phases have the $n = 2$ Ruddlesden−Popper structure, is shown in Figure 2c. The reduction in the Bragg *R* factor (R_B) is comparable with the single-phase model with inclusion of strain broadening. However, the shoulders on many peaks are now correctly predicted. A two-phase model in which the second phase is a $n = \infty$ perovskite was not successful in improving the fit. The refinements with two Ruddlesden−Popper phases were successful for the $Sr_2LnMn_2O_7$ compounds where Ln = La−Gd. The lattice parameters for the two phases present in each sample are given in Table 3. The two-phase behavior appears dependent on the precise thermal treatment to which the samples are exposed, particularly with respect to the phase fractions. For example, two batches of $Sr_2NdMn_2O_7$ gave very similar lattice parameters (Batch 1: phase 1: $a = 3.8483(2)$ Å, $c = 20.018(2)$ Å, phase 2: $a = 3.8511(1)$ Å, $c = 19.9567(9)$ Å, compared with batch 2: phase 1: $a = 3.8497(3)$ Å, $c = 20.009(2)$ Å, phase 2: $a = 3.8508(2)$ Å, $c = 19.958(1)$ Å) but the first batch produced a 7/3 ratio of the two phases, whereas the second batch contained equal amounts of both. This significant change may have been caused by small differences in the firing times (batch 2 final firing for 5 rather than 4 days at 1300 °C in air). The extent of phase separation is thus increased after the optimal heating time has been exceeded.

Table 1. Sample Preparation Conditions for $Sr_2LnMn_2O_7$ (Ln = Lanthanide)[a]

compound	1350 °C (air)	1450 °C (air)
$Sr_2LaMn_2O_7$	96	
$Sr_2PrMn_2O_7$	225	
$Sr_2NdMn_2O_7$	120*	
$Sr_2SmMn_2O_7$	400	
$Sr_2EuMn_2O_7$	300	
$Sr_2GdMn_2O_7$	200	
$Sr_2TbMn_2O_7$	200	
$Sr_2DyMn_2O_7$	250	
$Sr_2HoMn_2O_7$	300	
$Sr_2ErMn_2O_7$	100	50
$Sr_2YMn_2O_7$	450	50

[a] Reaction times are given in hours. All compounds were initially fired at 800, 1000, and 1200 °C for 24 h at each temperature in air. * indicates a 1300 °C reaction temperature.

Table 2. Sample Preparation Conditions for $Sr_{2-x}Ln_{1+x}Mn_2O_7$ (Ln = Nd^{3+}, Tb^{3+})[a]

x	1300 °C (air)	1350 °C (air)	1350 °C (N_2)
		$Sr_{2-x}Tb_{1+x}Mn_2O_7$	
0.1		240	96
0.3		240	120
0.5		48	120
		$Sr_{2-x}Nd_{1+x}Mn_2O_7$	
0.05	120		
0.1	72		
0.15	120		
0.2	96		
0.3	144		
0.4	144	96	96
0.5	168	96	96

[a] Reaction times are given in hours. All compounds were initially fired at 800, 1000, and 1200 °C for 24 h at each temperature in air.

An example of the Rietveld fit to a two-phase model is shown in Figure 3 for $Sr_2EuMn_2O_7$. The {0 0 10} reflection in $Sr_2PrMn_2O_7$ (where the multiphasic nature is most marked) has a second shoulder at higher angle from the main peak, as shown in Figure 2. Although incorporation of a third Ruddlesden−Popper phase improved the fit, only the lattice parameters were found to be stable in the refinement. This material is being further investigated with the use of synchrotron data. None of the other compounds contained this third phase, and therefore a three-phase model will not be included in this general discussion.

Inclusion of a second phase into the refinements of the $Sr_2LnMn_2O_7$ patterns (Ln = Tb−Er) led either to unstable refinements with one of the phase fractions converging to zero or the refinement of unphysical bond distances with large standard deviations. In all cases, Ln = Tb−Er, there is no direct evidence from inspection of the single-phase fits, for example, the shoulder on the {0 0 10} reflection seen for the larger lanthanides, that two phases are present. The single-phase Rietveld fit to $Sr_2YMn_2O_7$ is shown in Figure 4. Although the X-ray patterns of $Sr_2LnMn_2O_7$ for Ln = Tb−Er, Y were clearly those from single phases at the resolution of our diffractometer, with no problems in fitting the peak shape, the intensity fit to certain weak reflections was inadequate from a model with a statistical distribution of both A cations over the two available sites. This is most pronounced for the {103} reflection at 27° 2θ, which is strongly dependent on the difference between

(27) Drofenik, M.; Golic, L. *J. Cryst. Growth* **1973**, *21*, 305.
(28) Lucchine, E.; Minichelli, D.; Sloccari, G. *Acta Crystallogr. B* **1973**, *29*, 2356.
(29) LeBail, A. *Mater. Res. B.* **1988**, *23*, 447.
(30) Rodriguez-Carvajal, J.; Fernandez-Diaz, M. T.; Martinez, J. L. *J. Phys. Condensed Matter* **1991**, *3*, 3215.

Table 3. Cell Parameters for $Sr_2LnMn_2O_7$ and $Sr_{2-x}Ln_{1+x}Mn_2O_7$ Derived from Rietveld Refinements[a]

	$Sr_2LnMn_2O_7$			
	phase one		phase two	
Ln	*a* (Å)	*c* (Å)	*a* (Å)	*c* (Å)
La	3.87558(25)	19.9902(12)	3.87527(29)	20.0136(12)
Pr	3.85547(25)	20.0256(16)	3.85660(14)	19.9779(8)
Nd	3.84970(25)	20.0089(16)	3.85081(20)	19.9582(12)
Sm	3.83870(26)	19.9504(20)	3.83997(22)	19.9107(15)
Eu	3.83079(13)	19.9847(11)	3.83402(15)	19.9444(13)
Gd	3.82729(17)	19.9880(14)	3.82951(23)	19.9531(18)
Tb	3.82060(14)	19.9847(8)		
Dy	3.82080(6)	19.9462(4)		
Ho	3.82206(5)	19.8950(3)		
Y	3.82196(7)	19.8969(4)		
Er	3.82254(4)	19.84723(3)		

	$Sr_{2-x}Nd_{1+x}Mn_2O_7$			
	phase one		phase two	
x	*a* (Å)	*c* (Å)	*a* (Å)	*c* (Å)
0.1	3.84695(15)	20.03468(98)	3.84475(18)	20.17819(142)
0.2	3.84275(12)	20.11771(91)	3.84097(12)	20.15395(100)
0.3	3.84120(27)	20.16618(258)	3.83832(7)	20.19907(60)
0.4	3.84323(5)	20.28800(45)		
0.5	3.84107(12)	20.31873(74)		

	$Sr_{2-x}Tb_{1+x}Mn_2O_7$			
	phase one		phase two	
x	*a* (Å)	*c* (Å)	*a* (Å)	*c* (Å)
0.1	3.82082(10)	20.10471(60)		
0.2	3.81995(11)	20.10348(69)		
0.3	3.82424(10)	20.12391(89)	3.82679(19)	20.09614(167)
0.5	3.83417(19)	20.00589(151)	3.83829(14)	19.97793(96)

[a] Where no data for a second phase are given, the pattern was refined using a monophasic model

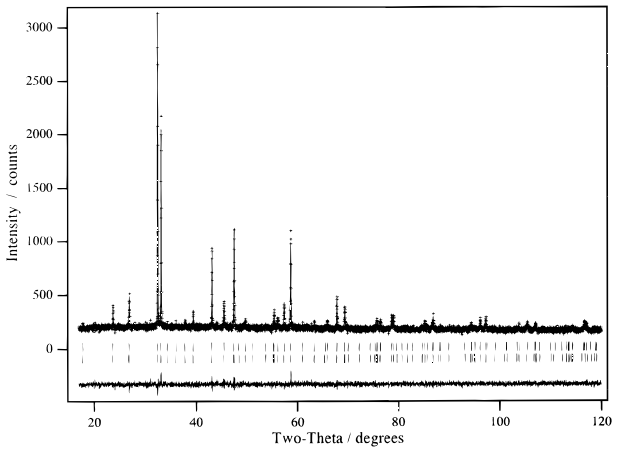

Figure 3. Rietveld refinement of $Sr_2EuMn_2O_7$ at room temperature using a two-phase model ($wR_p = 7.20\%$, $R_p = 5.74\%$, and $\chi^2 = 1.06$). The fit is shown as in Figure 2. The lower ticks represent phase one (as defined in Table 3); the upper ticks represent phase two.

the average scattering factors on the two cation sites. Refinement was then carried out with a model which distributed the two cations unequally between the rock-salt and perovskite A sites, conserving the overall composition. The {103} reflection is shown in Figure 5 for $Sr_2DyMn_2O_7$ to demonstrate the improvement gained by inclusion of a cation ordered model. These refinements revealed an increasing tendency in the single-phase samples for preferential occupancy of the site in the perovskite block by the Sr^{2+} cation as the size of the Ln^{3+} cation decreases (Figure 6; Y^{3+} is isoelectronic

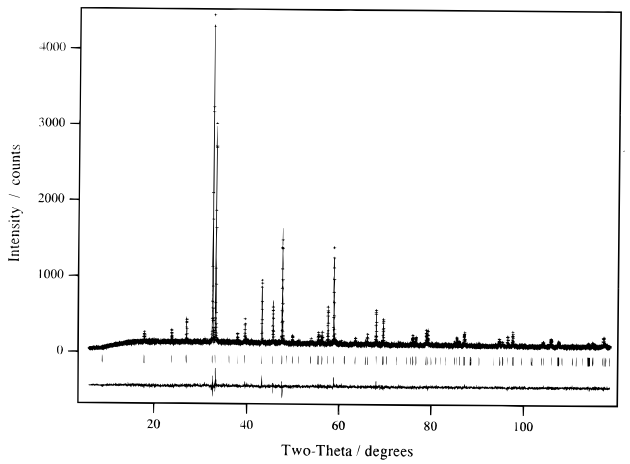

Figure 4. Rietveld refinement of $Sr_2YMn_2O_7$ at room temperature using a single-phase model ($wR_p = 9.43\%$, $R_p = 7.37\%$, and $\chi^2 = 1.18$). The observed data are given as points, the fit is a solid line, and the difference is shown below on the same scale. The ticks indicate the positions of the Bragg reflections.

with Sr^{2+} and hence X-rays are insensitive to any ordering in $Sr_2YMn_2O_7$). In the two-phase refinements (Ln = La−Gd), each phase was initially allowed to have different degrees of ordering, while conserving the same overall composition for each phase. This resulted in refinement to identical values for the site occupancy in both phases in all cases: site occupancies were then therefore constrained to be the same in both phases to improve stability. The crossover to single-phase behavior appears strongly correlated with the onset of the A cation ordering. This cation ordering increases less markedly beyond terbium and reaches its maximum extent (95.0(8)%) at erbium. For the larger lanthanides, a more gradual change in occupancy is observed as a function of cation size. The unit cell volumes and lattice parameters for the $Sr_2LnMn_2O_7$ phases are shown in Figures 7 and 8.

For Ln = Nd, Tb, we explored the variation of the Ln/Sr ratio to investigate the stabilization of other manganese oxidation states in the $n = 2$ RP structure. Rietveld refinement of other lanthanide compositions in the $Sr_{2-x}Ln_{1+x}Mn_2O_7$ ($0 \le x \le 0.5$) series reveals that the tendency to form two phases is more subtly dependent on the reaction conditions than in the $Sr_2LnMn_2O_7$ series. For example, $Sr_{1.4}Nd_{1.6}Mn_2O_7$ exhibits two $n = 2$ RP phases after reaction for 2 days under N_2 but is single phase after 4 days, despite no impurity peaks from the starting materials being evident at the earlier stage. The extent of ordering of the Nd^{3+} cations on the rock-salt site increases with higher Nd content from 64% at $x = 0.0$ to 79% at $x = 0.5$, with the Sr preferentially located in the perovskite block. The $Sr_{2-x}Nd_{1+x}Mn_2O_7$ series becomes single phase for $x > 0.3$ as the extent of ordering increases. The cell parameters for these phases are shown in Figure 9 and Table 3. In contrast, the $Sr_{2-x}Tb_{1+x}Mn_2O_7$ compounds (Figure 10, Table 3) are single phase and ordered for $x = 0.0$ and 0.1 but become biphasic for $0.3 \le x \le 0.5$, demonstrating the complex relationship between cation ordering and phase separation. In an effort to isolate truly single phases for the biphasic compositions discussed above, extended heating times at the highest possible reaction temperatures were investigated. It

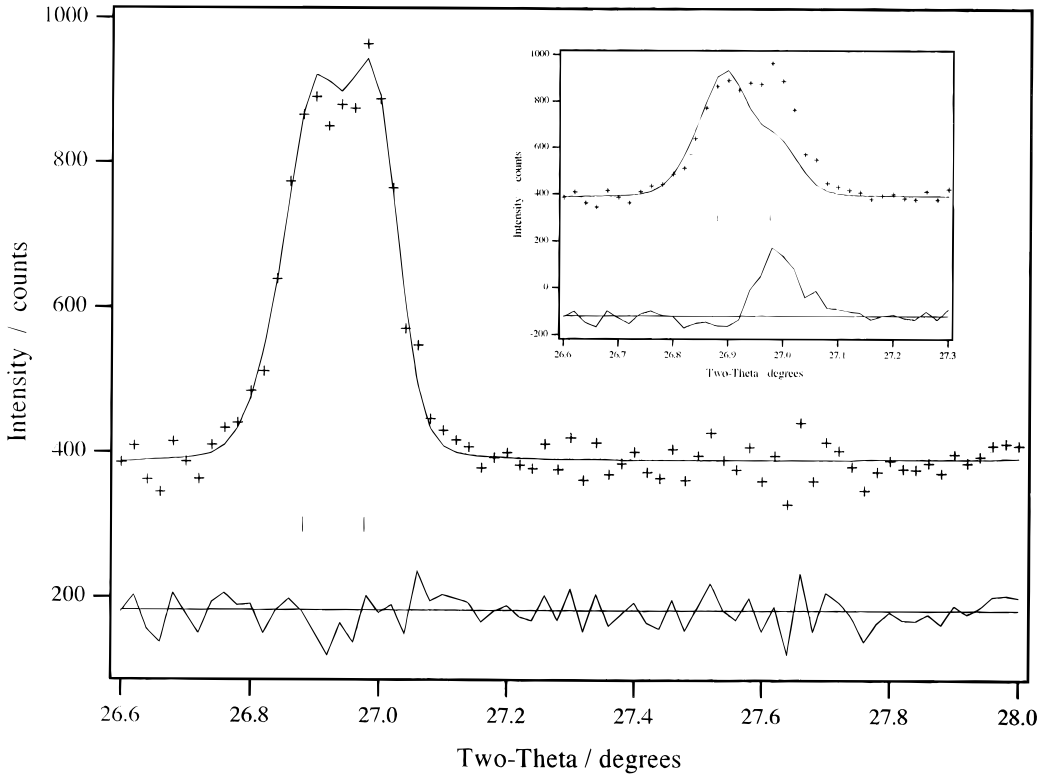

Figure 5. The {1 0 3} reflection of the $n = 2$ Ruddlesden−Popper phase; $Sr_2DyMn_2O_7$. The figure demonstrates the improvement in the fit which occurs when ordering of Dy^{3+} and Sr^{2+} between the two available A cation sites is introduced. The inset shows the fit with a completely disordered model ($wR_p = 5.44\%$, $R_p = 4.17\%$, and $\chi^2 = 1.44$ compared with $wR_p = 5.16\%$, $R_p = 4.03\%$, and $\chi^2 = 1.30$ for the ordered model shown in the main figure).

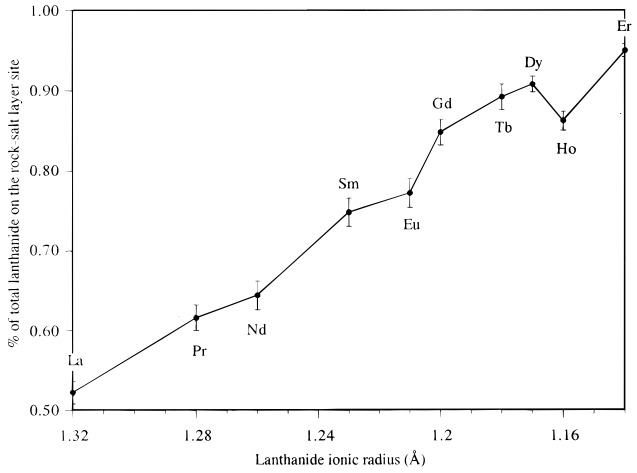

Figure 6. Percentage of the Ln^{3+} cations occupying the A cation site in the rock-salt layer in the $Sr_2LnMn_2O_7$ phases shown as a function of lanthanide cation radius (the lanthanides are shown in the order La−Er, and hence the abscissa decreases from left to right). The eight coordinate radii of Shannon and Prewitt are used.[34] A cation-disordered phase would have 67% occupancy of this site.

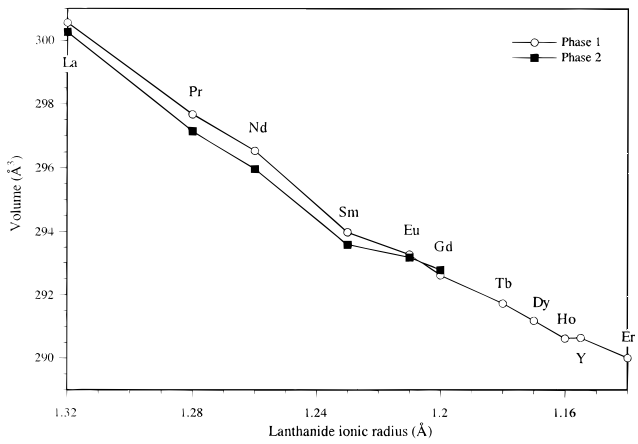

Figure 7. Unit-cell volume as a function of the Ln^{3+} lanthanide cation radius for the $Sr_2LnMn_2O_7$ phases. The volumes of both phases are shown for the biphasic samples.

appears from these experiments that the $n = 2$ RP phase decomposes irreversibly into the $n = \infty$ perovskite phase on prolonged heating (17 days in air at 1300 °C for $Sr_{1.9}Nd_{1.1}Mn_2O_7$).

Discussion

The present study of the synthesis and crystal chemistry of the $n = 2$ Ruddlesden−Popper manganates reveals important details concerning the phase purity and cation distribution which are important for tuning the Mn−Mn interaction via the oxygen framework and thus influencing the electronic properties. This crystal chemistry appears qualitatively different from the previously investigated $n = 1$ and $n = \infty$ manganates. There are two notable points resulting from the detailed study of the Rietveld refinements of the new phases prepared here. First, the cation ordering in the Ruddlesden−Popper structure for the smaller lanthanides in $Sr_2LnMn_2O_7$, seen to a lesser extent with increasing x in the $Sr_{2-x}Nd_{1+x}Mn_2O_7$ series, and second, the separation into two phases for the larger lanthanides. This phase separation was initially indicated by high-resolution powder neutron diffraction studies of $SrNd_2Mn_2O_7$, where precise Mn−O bond lengths can be refined in the two separate phases.[16,24] The phase

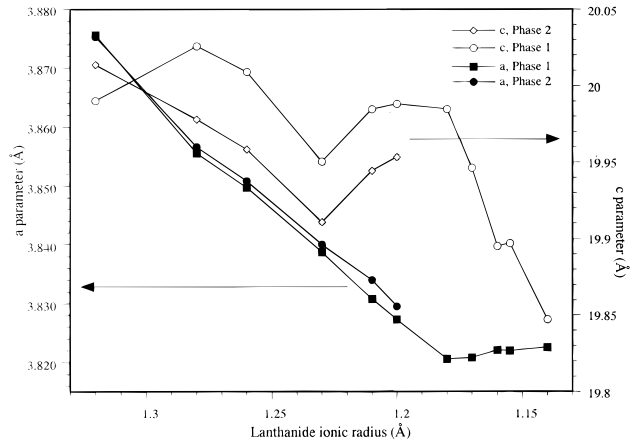

Figure 8. Unit-cell parameters for the $Sr_2LnMn_2O_7$ series as a function of the lanthanide cation. *a*, phase 1,*c*, phase 1 and *a*, phase 2,*c*, phase 2 are the lattice parameters of the first and second phases present in the biphasic samples.

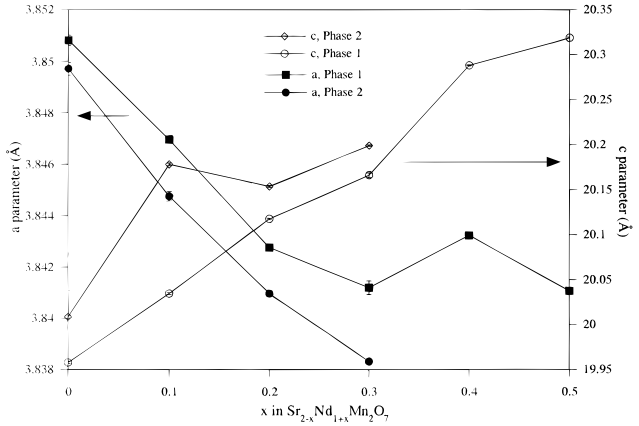

Figure 9. Unit-cell parameters for the $Sr_{2-x}Nd_{1+x}Mn_2O_7$ phases ($0 \leq x \leq 0.5$). Biphasic samples are depicted as in Figure 8.

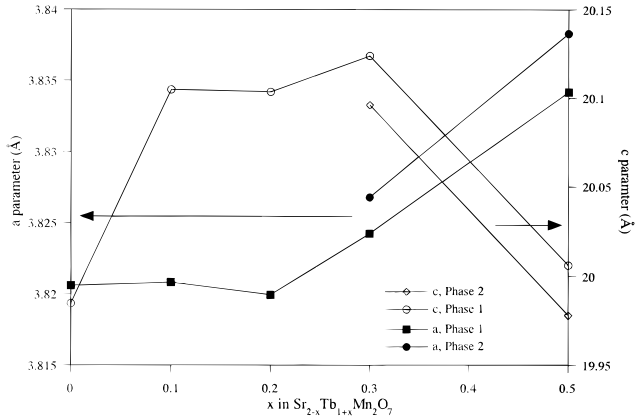

Figure 10. Unit-cell parameters for the $Sr_{2-x}Tb_{1+x}Mn_2O_7$ phases ($0 \leq x \leq 0.5$). Biphasic samples are depicted as in Figure 8.

coexistence at the $Sr_2LnMn_2O_7$ composition occurs for those lanthanide cations for which preferential segregation of the Ln^{3+} cations onto the smaller nine-coordinate site in the rock-salt layer does not occur. The unsuccessful attempt to include microstrain into a single-phase model, and the clear shoulders on several reflections, points to the presence of discrete phases, rather than a distribution of lattice parameters. The details of the phase separation for a given lanthanide appear dependent on the synthesis conditions, and it may be that a single phase $n = 2$ material of composition $Sr_2LnMn_2O_7$ can be prepared under very well-defined reaction conditions: what is clear from the current study is that the formation of such single phases is much more difficult to achieve for the larger lanthanides. The details of the structures of the two phases are inaccessible from the current refinements, but the lattice parameters and unit cell volumes vary in a similar way for the two phases. It is interesting to note that the unit-cell volumes are very similar for the two phases despite the difference in *a* and *c*. This may indicate that Sr/Ln segregation is not responsible for the phase separation and is evidence for the homogeneity of the samples: no significant variation in the Sr/Ln ratio was detected by the energy-dispersive X-ray analysis for the samples studied here. The differences between the two phases are discussed more fully in ref 24 on the basis of powder neutron diffraction data. We expect electron microscopy studies, presently underway, to throw more light on this issue. Until these studies are complete, we cannot totally rule out the possibility that extended defects are present in our samples.

In the case of biphasic $Sr_{1.9}Nd_{1.1}Mn_2O_7$, there appears to be an optimal firing time before the more thermodynamically stable perovskite forms. This decomposition represents the extreme case of the formation of intergrowths which are well-known in this type of layered material.[31] The decomposition of $Sr_2SmMn_2O_7$ at temperatures above 1400 °C indicates that reaction temperature must also be chosen carefully for the isolation of the metastable $n = 2$ phases.

The ordering of the lanthanide cation onto the smaller nine-coordinate site in the rock-salt layer appears to be the key crystal-chemical factor in allowing the isolation of pure single phases under the reaction conditions studied here. The percentage of the Ln^{3+} cations that occupy the site in the rock salt layer is shown in Figure 6. The metal−oxygen bond lengths around the two different cation sites in the single-phase cation ordered material $Sr_2DyMn_2O_7$ clearly reveal the difference in effective size of the two available sites which is the driving force for the ordering—(nine-coordinate rock-salt site Dy/Sr−O distances 4 × 2.728(2) Å, 1 × 2.29(2) Å, 4 × 2.545(8) Å: 12-coordinate perovskite site 4 × 2.70172 (4) Å, 8 × 2.746(9) Å), though the absolute values clearly need to be treated with caution in view of the use of powder X-ray diffraction to refine them. The refined parameters for the $Sr_2DyMn_2O_7$ phase are given in Table 4. The refinement of the two-phase $Sr_2LaMn_2O_7$

Table 4. Refined Parameters for $Sr_2DyMn_2O_7$ at Room Temperature Using a Single-Phase Model[a]

	x/a	*y/b*	*z/c*	occupancy
Sr(1)	0	0	0.5	0.92(1)
Dy(1)	0	0	0.5	0.08(1)
Sr(2)	0.5	0.5	0.18324(9)	0.546(5)
Dy(2)	0.5	0.5	0.18324(9)	0.454(5)
Mn	0	0	0.09777(23)	1
O(1)	0	0	0	1
O(2)	0	0	0.20211(73)	1
O(3)	0	0.5	0.09891(60)	1

[a] The refinement was carried out using a fixed overall isotropic thermal factor, U_{iso}, of 0.001 Å^2, giving $wR_p = 5.16\%$, $R_p = 4.03\%$, and $\chi^2 = 1.30$.

(31) Fu, W. T.; Zandbergen, H. W.; Xu, Q.; VanRuitenbeek, J. M.; DeJongh, L. J.; vanTendeloo, G. *Solid State Commun.* **1989**, *70*, 1117.

sample shows that the La^{3+} cation, which is the largest trivalent cation in this study, prefers the 12-coordinate site. This indicates a competition between charge and size effects. The perovskite layer site is more favorable for highly charged cations when size effects are not dominant.

Cation ordering of this type has been observed in a single-crystal X-ray diffraction study of the isostructural bismuthate $Ba_{1.7}K_{1.3}Bi_2O_7$, where all of the K atoms are situated in the 9-coordinated rock salt layer site,[32] in the same $I4/mmm$ space group. No evidence was found for a lowering of symmetry in any of the $Sr_2LnMn_2O_7$ samples studied, though high-resolution neutron diffraction will be needed to confirm this. Cation ordering is accompanied by symmetry-lowering to $P4_2/mnm$ in $SrTb_2Fe_2O_7$.[33] The existence of the two distinct A cation sites in the $n = 2$ Ruddlesden−Popper structure gives the ability to order the cations between the two distinct sites as the average cation size is reduced. This contrasts with the single A site in the $n = \infty$ perovskites, where tilting of the BO_6 octahedra is required to reduce the coordination number of the A site as the cation becomes smaller, leading to a variety of structure types.

For the $Sr_2LnMn_2O_7$ series, it is interesting to note that the volume of each phase, in the two-phase compounds (Figure 7) is very similar and follows the same trends. Phase two consistently has a larger *a* and smaller *c* parameter than phase one. The fraction of these two phases changes as a function of lanthanide size such that the "large *c*-axis" phase becomes predominant with decreasing lanthanide size, until a single phase is formed from terbium onward. The volumes of all the phases decrease smoothly as expected with the lanthanide radius. The dependence of the lattice parameters on the radius of the Ln^{3+} cation is shown in Figure 8. The *a* parameter for both phases falls rapidly on reduction of the average cation size from La to Tb and is then constant across the single-phase region. This establishes a minimum Mn−O(3) bond length of around 1.91 Å for manganese in this coordination and oxidation state, and for bond lengths above this value the cell dimensions are governed by the average size of the A cations. The *c* parameter shows an anomalous rise for the compounds (Sm−Tb) which are partially ordered, until the expected decrease with reduced average cation size is seen in the single phase samples from Tb to Er. The *c* parameter starts to decrease only when *a* reaches its minimum value. The overall behavior can be understood in terms of the anisotropy of the layered structure—the initial contraction in the *a* parameter is driven by the tolerance factor in the MnO perovskite blocks until a minimum bond length is reached and the *c* parameter then decreases to produce the required reduction in volume. While the volume variation is smooth, the anomaly in the *c*/*a* ratio at the partially ordered phases may reflect details of the cation distribution over the two sites which are inaccessible from the current refinements.

In both the $Sr_{2-x}Nd_{1+x}Mn_2O_7$ and $Sr_{2-x}Tb_{1+x}Mn_2O_7$ series, the nonmonotonic variation of the lattice parameters (Figures 9 and 10, respectively) and unit-cell volume reflects the competition between the smaller size of the Tb^{3+} or Nd^{3+} cations substituted for Sr^{2+}, the increase in size at the B site as reduction occurs from Mn^{IV} to Mn^{III}, and the dependence of phase separation on the overall composition. For $Sr_{2-x}Tb_{1+x}Mn_2O_7$, the volume reaches a maximum at $x = 0.3$, corresponding to the single-phase materials, and decreases slightly at $x = 0.5$. As the lattice parameter *a* has reached its minimum value at $Sr_2TbMn_2O_7$, the increase in size on reduction to Mn^{III} causes *a* to increase monotonically. The *c* parameter reaches a maximum at $x = 0.3$ corresponding to the maximum in the volume and then decreases as phase separation becomes apparent. In all three families studied, single phases are accessible only under the current conditions when the *a* parameter has reached its minimum value. When multiphase behavior occurs in this manganate Ruddlesden−Popper series, simple visual inspection of the powder X-ray pattern is insufficient to identify the phase separation. Comparison of the Rietveld fits to both single- and two-phase models is required to assess the outcome of syntheses.

The recent observation of both conventional and unconventional CMR (i.e., associated and not associated with bulk ferromagnetism, respectively) in the $n = 2$ Ruddlesden−Popper manganates[16,22] requires a detailed understanding of the crystal structures and chemistry of these compounds if the origins of the magnetoresistance are to be understood. It is clear that the synthesis of truly single phases for a wide range of oxidation states is not straightforward in this structure type: phase separation into two similar $n = 2$ RP phases is a previously unsuspected problem for the known materials. There is a pronounced dependence both of the crystal structure and the ease of synthesis of single phases on the size of the lanthanide cation and the manganese oxidation state in question. The patterns of cation ordering and the dependence of lattice parameters and cell volumes on manganese oxidation state may well be important in both understanding the differences in properties from the perovskites and opening the way to the effective manipulation of the magnetotransport via the dimensionality of the Mn−O network.

Acknowledgment. We acknowledge financial support from the EPSRC and the donors of the Petroleum Research Fund, administered by the American Chemical Society. We thank Dr. P. G. Radaelli (Institut Laue-Langevin) for his involvement in the initial two phase refinements of powder neutron diffraction data on $Sr_{2-x}Nd_{1+x}Mn_2O_7$, and Dr. D. E. Cox (Brookhaven National Laboratory) for performing preliminary diffraction experiments on $Sr_2LaMn_2O_7$ at NSLS.

CM960398R

(32) Cava, R. J.; Siegrist, T.; Peck Jr., W. F.; Krajewski, J. J.; Batlogg, B.; Rosamilia, J. *Phys. Rev. B* **1991**, *44*, 9746.
(33) Samaras, D.; Collomb, A.; Joubert, J. C. *J. Solid State Chem.* **1973**, *7*, 337.
(34) Shannon, R. D.; Prewitt, C. T. *Acta Crystallogr.* **1969**, *B25*, 925.